Journal of Materials Science: Materials in Electronics (2019) 30:2057–2066
https://doi.org/10.1007/s10854-018-0477-z

Enhancing the photovoltaic performance of perovskite solar cells by potassium ions doping

Shan Jia[1] · Jinfeng Wang[1] · Lei Zhu[1]

Received: 12 August 2018 / Accepted: 28 November 2018 / Published online: 14 December 2018

Abstract
Organometal halide perovskite solar cells (PSCs) have attracted much attention due to their high photovoltaic efficiency and low fabrication cost. The perovskite layer plays a critical role on the power conversion efficiency (PCE). The main issues in perovskite layer are the coverage and crystallinity of perovskite grain based on substrate. Here, potassium ions were doped into perovskite layer to improve the growth, structure, properties of perovskite films and the photovoltaic performance of PSCs. The potassium ions significantly affect the J_{sc} and efficiency but affect the V_{oc} slightly. The J_{sc} increases from 14.73 to 19.98 mA cm^{-2}, and the efficiency increases from 10.16 to 13.57% at the doping level of 0.5% (molar ratio). The incorporation of potassium ions into perovskite also affects the crystallisation and morphology of the perovskite films and thus the PCE of PSCs. The crystallinity and denseness of perovskite film are enhanced and crystallite size is enlarged after potassium ions are doped into perovskite layer. At the same time, hysteresis free and stable device is obtained with the PSC at the doping level of 0.5% of potassium ions (molar ratio).

1 Introduction

Methylammoniun lead halide perovskite solar cells (PSCs) have attracted much attention due to their high photovoltaic efficiency and low fabrication cost. The outstanding photovoltaic is related to the unique characters of perovskite, such as optimal band gaps (1.55 eV), high absorption coefficients (~ 10^4 cm^{-1}), high charge carrier mobility (10–10^2 cm^2 V^{-1} s^{-1}) and long charge carrier diffusion length (10^2–10^5 nm) [1–5]. Great process of efficiency has been made in PSCs since 3.8% in 2009 to the current record efficiency of 22.1% [6]. The fast improvement of efficiency is due to the development of the processing technology. The high quality perovskite film should possess full surface coverge, large crystal size and low defect density. Driven by improvement of the quality of perovskite thin film, various processing technologies such as vacuum deposition, high temperature process and solution process have been rapidly developed. Due to low cost, solution processes such as spin-coating, slot-die coating, blade-coating and spray coating have widely been used [7–10]. Meantime, solution process method is usually followed by two-step method and one-step method. For two-step method [11], the CH_3NH_3I is coated on the substrate and then deposited by PbI_2. For one-step method [12], a mixture solution of CH_3NH_3I and PbI_2 is coated on the substrate directly.

Based on the cheapest spin-coating method, ion doping process has also been rapidly developed in recent years. For instance, the band gap and electronic property of methylammonium lead halide perovskite can be tailored by incorporating metal cations Sn^{2+} [13, 14], inorganic halide anions such as Br and Cl [15, 16], or organic cations such as methylammonium and formamidinium [17, 18]. Snaith's group pioneer in using the precursor solutions to obtain the high quality $MAPbI_{3-x}Cl_x$ perovskite absorber that has an electron–hole diffusion length of over 1 μm [19]. The long diffusion length can ensure efficient transport that implies the photo generated charges can reach the corresponding electrode interfaces without much charges loss. Grätzel and his colleagues prepared $FA_xMA_{1-x}PbI_3$ perovskite by the sequential method and found that the photocurrent onset was shifted by 20 nm to the red from 780 to 800 nm, resulting in power conversion efficiency of up to 14.9% [20]. Noel

Electronic supplementary material The online version of this article (https://doi.org/10.1007/s10854-018-0477-z) contains supplementary material, which is available to authorized users.

✉ Lei Zhu
lzhu@cumt.edu.cn

[1] School of Materials Science and Engineering, China University of Mining and Technology, Xuzhou 221116, China

et al. reported the completely lead-free $MASnI_3$ perovskite solar cell processed on a mesoporous TiO_2 scaffold, reaching efficiency of over 6% under 1 sun illumination firstly [21]. The efficiency value was lower than that of $MAPbI_3$ owing to the recombination with self-doping carriers. However, the device of open circuit voltages achieved over 0.88 V resulting from a material which has a 1.23 eV band gap.

Besides, some alkali metal cations are also suitable additive in perovskite solar cell. For alkali metal doped into perovskites, several studies have been reported previously. Liu et al. demonstrated the excellent photovoltaic performance with the PCE up to 13.7% and superior humidity stability of two-dimensional perovskite solar cell achieved by doping Cesium cations [22]. Snaith et al. introduced aluminium acetylacetonate to the perovskite precursor solution and demonstrated that incorporating impurity aluminum cation into perovskite could enhance the crystal quality by reducing the microstrain in the polycrystalline film and reduce the non-radiative recombination rate [23]. As a result, the PCE of 19.1% with negligible hysteresis in planar heterojunction solar cell was obtained by doping aluminum cation. Several additives in IA group element, including potassium, Natrium and Lithium cations (e.g. KCl, NaCl, and LiCl), can be used to form smooth, continuous, and uniform films with flawless perovskite nanocrystals. Chu et al. explored the effect of salt additives (KCl, NaCl, LiCl) for perovskite solar cells and found that a small amount of KCl as an additive had a significant enhancement in PCE from 11.40 to 15.08% [24]. Chang et al. also demonstrated that Na^+ or K^+ can enhance the grain size of the perovskite and improve the charge carrier lifetime [25].

In this study, we investigated the influence of potassium metal halides as additives on the performance of perovskite solar cells. In order to eliminate the interference factor of Cl element, KI is used in this manuscript rather than KCl reported in other literature. The structure of fabricated solar cell is mesoporous structure which is different with invert planar structure reported in other literature. Based on more convenient one-step spin-coating method, we incorporated potassium metal halides into the perovskite layer and found that the incorporation of potassium ions into $MAPbI_3$ affected the J_{sc} and efficiency significantly but affected the V_{oc} slightly. The J_{sc} increased from 14.73 mA cm^{-2} to 19.98 mA cm^{-2} and the efficiency increased from 10.16 to 13.57% at the doping level of 0.5%. The incorporation of potassium ions into $MAPbI_3$ perovskite layer also affected the crystallisation and morphology of the perovskite films and thus the PCE of PSCs. A hysteresis free PSC was obtained based on mesoporous structure device with PCE of 13.52% (reverse scan) and 13.39% (forward scan) with optimal doping content of potassium ions. The device incorporation with potassium ions exhibited longer stability over 18 days under ambient air (46 RH%) without encapsulation.

2 Experimental section

2.1 CH_3NH_3I synthesis

CH_3NH_3I (MAI) was synthesized from mixing the CH_3NH_2 solution and the HI solution by 1:1 molar ratio in a round-bottom flask at 0 °C for 2 h under stirring. The solvent was evaporated and the precipitate was washed with diethyl ether. The precipitate was dried at 60 °C for 24 h in a vacuum oven.

2.2 Perovskite fabrication

Fluorine-doped tin oxide (FTO, Pilkington, TEC 15) glass substrate was partially etched with Zn powder and 2 M HCl to form the electrode pattern. Then, the substrate was cleaned with deionized water, ethanol, isopropanol and absolute ethyl alcohol for 20 min, respectively. A 50-nm-thick dense blocking TiO_2 was deposited via spin coated method, which was followed by a heating process at 450 °C for 30 min. For the mesoporous TiO_2 film, TiO_2 paste (Dyesol, 18 NRT) was mixed with absolute ethanol in the ratio 1:5.5 (weight ratio), which was spin coated on the substrate at 5000 rpm for 30 s, then dried at 130 °C for 10 min and annealed at 500 °C in air for 15 min. Perovskite layer was deposited by using one-step method reported in the literature [26]. After substrate was cooled down to room temperature, perovskite precursor solutions were spin coated on mesoporous TiO_2 films at 1000 rpm for 10 s and then at 5000 rpm for 30 s. The 1 mL toluene was dropped on the revolving substrate at 5000 rpm for 15 s. The dropping speed was 1/8 mL s^{-1}. The spin-coated perovskite films were then annealed at 110 °C for 10 min then at 130 °C for 5 min. The perovskite precursor solution was prepared by mixing PbI_2 (Alfa), MAI and KI in 1 mL dimethyl sulphoxide (DMSO). The specific quality of the various ingredients is shown in Table S1. Note that the mixture solution was agitated and heated for 2 h at 75 °C in glove box. The hole transporting layer (HTL) was deposited by spin coating at 3000 rpm for 30 s. The HTL precursor was synthesized by spiro-OMeTAD powder (72.3 mg) with additives of 17.5 uL Li-bis(trifluoromethanesulfonyl) imide (Li-TFSI), 28.8 uL 4-*tert*-butylpyridine (TBP) and 1 mL chlorobenzol. Finally, 50 nm thick Ag was thermally evaporated on top of the device to form the back contact. The active area of device was 10 mm^2 determined by a black mask with dimensions of 2 mm × 5 mm.

2.3 Characterization

The morphology, crystal structure, photoluminescence (PL) and Time-resolved PL (TR-PL) spectra of TiO_2/$MAPbI_3$

films were characterized by a field emission scanning electron microscope (FESEM, S-4800, Hitachi, Japan), an X-ray diffraction (XRD, DX-2700B), a steady state fluorescence spectrophotometer (Cary 300, Varian, USA) spectrometer and a lifetime state spectrometer (FLS 980, Edinburgh instruments). UV–vis spectrophotometer (Cary 300, Varian, USA) was employed to characterize the diffusion absorption spectra. Photocurrent–voltage (J–V) curves of perovskite solar cells were characterized by a Keithley 2420 Source Meter under solar illumination (100 mW cm^{-2}, Oriel Sol 3A, Newport) which was calibrated by a standard silicon solar cell (Oriel Instrument). The incident photon to current conversion efficiency (IPCE) was measured by using a power source (Newport 300 W Xenon lamp, 66902) with a monochromator (Newport Cornerstone 260) and a power meter (Newport 2936-C). Element types and distribution were measured using Electron probe micro-analyzer (EPMA-8050G). Instrument model of X-Ray photoelectron spectrometer (XPS) is ESCALAB 250Xi (Thermo Fisher, USA).

3 Results and discussion

To understand the effects of the additives on the perovskite structure based on the one-step spin-coating method, X-ray diffraction (XRD) measurements were conducted to investigate crystal structure variation of the perovskite film made with a range of K^+ doped concentrations up to 1.0%. In Fig. 1a, all the perovskite films show the character diffraction peaks of perovskite, which are verified by the dominant diffraction peaks at 14.2°, 28.5°, corresponding to the reflections from (110), (220), respectively. In addition, the diffraction peak of PbI_2 is not detected at $2\theta = 12.7°$, which means excellent crystallinity and high level of phase purity of the perovskite film. All samples crystallise in a typical tetragonal crystal structure as reported previously, it demonstrates that K^+ has no obvious effect on crystal structure. The intensities of perovskite peaks (110) and (220) are enhanced significantly as the doping level increases up to 0.5%. The intensities of the dominant perovskite (110) and (220) peaks increase substantially but there is no obvious shift in the position of the diffraction peaks. The potassium ion might be predominantly expelled to the perovskite surface and grain boundaries during crystallisation, which might enhance the crystalline of perovskite. Considering the unconspicuous shift of the diffraction peaks, the reason may be that the ionic radii of K^+ (138 pm) is much smaller than that of MA^+ (217 pm), which makes K^+ unlikely to substitute MA^+ within the perovskite crystal lattice. Otherwise, the 2θ will change significantly, which will be further discussed later. It shows the corresponding magnified XRD patterns in the region of 13.8°–14.8° in Fig. 1b. The slight left-shift of the XRD patterns at (110) planes by 0.08°, might result from the void space with the octahedral crystal lattice partially filled with the smaller K^+. The corresponding magnified XRD patterns in the region of 28.2°–28.8° is shown in Fig. S1.

It has been reported that perovskite has two-dimensional or three-dimensional structure depending on the ion size [25]. The three-dimensional structure of $MAPbI_3$ would be distorted when it is doped with larger or smaller ions. According to the Goldschmidt tolerance factor: t, the effect of K^+ doped into the crystal structure of $MAPbI_3$ can be estimated. It is worth noting that there is the formula: $t = (r_A + r_X)/[2^{1/2}(r_B + r_X)]$, where r_A and r_B are effective ionic radii of the cations and r_X is the anion radius [27]. The perovskite has a three-dimensional structure when the t value is in the range of 0.7–1. For more stable structure, t value should approach value 1 as much as possible. There is Pb^{2+}

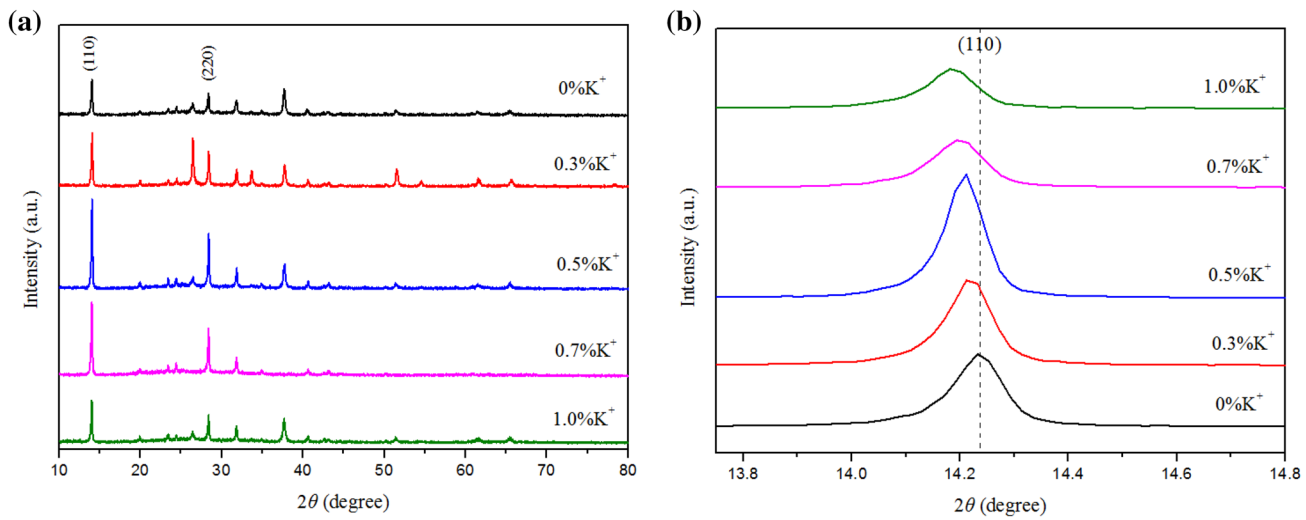

Fig. 1 **a** X-ray diffraction of perovskite in the region in 10°–80°. **b** The region magnified ranging from 13.8° to 14.8°

and I^- in the perovskite, resulting in the $r_B = r_{Pb}{}^{2+} = 0.119$ (nm), $r_X = r_I{}^- = 0.220$ (nm), t = 0.747 and t = 0.912 corresponding to $r_A = r_K{}^+ = 0.138$ (nm) and $r_A = r_{MA}{}^+ = 0.217$ (nm), respectively. The structure of perovskite with K^+ incorporated is distorted and unstable, which will be decomposed after annealing process. The result demonstrates that the K^+ prefers to enter the interstitial site rather than the substitutional sites in perovskite structure. Based on the above understanding of the position of K^+ in perovskite structure, a theoretical model is schematically illustrated in Fig. 2.

The absorption spectra of perovskite $MAPbI_3$ films with different doping degrees of K^+ is shown in Fig. 3a. Although all the films have the same thickness, the absorption of the perovskite thin film prepared with K^+ (0.5%) is greater than other films. The increased absorption intensity is attributed to the increase in the crystallinity and relatively greater surface coverage shown in Fig. 6. The corresponding magnified UV–visible absorption spectra in the region of 740–800 nm is showed in Fig. 3b. The absorption intensities increase substantially but there is no obvious shift in the position of the absorption onset. It demonstrates that the band gap of perovskite film has no significant change after doping potassium ions, which may result from the low doping degree. In order to show the change of absorption onset clearly, we put the right endpoints of absorption spectras at the same point in Fig. 3c. Compared with the reference films without K^+, a slight red shift of the absorption onset is observed when the sample is doped with K^+ (0.5% and 1.0%, respectively). All the perovskite thin films with the absorption onset around 780–790 nm exhibit wide absorption scopes from the ultraviolet range to the near-infrared wavelengths. The perovskite thin film doped with potassium ions (0.5%) exhibits absorption onset at 786 nm. The absorption onset corresponds to an optical band gap of 1.57 eV that is obtained from the intersection of the linear extrapolation of the edge of the absorption band and the horizontal axis. The specific calculation tangent chart is shown in Fig. 3d. It has been reported that the band gap of perovskite will be 1.72 eV after K^+ substitute MA^+ completely [25].

To study the charge extraction properties of the TiO_2 and perovskite layer with different doping concentrations, the analysis of PL was conducted separately. $MAPbI_3$ is a highly luminescent material, as a result, the quenching of its PL intensity is used as a measure of the charge extraction ability of the perovskite layer. The PL spectra of the perovskite deposited on mesoporous TiO_2/compacting TiO_2/nonconductive glass substrates is shown in Fig. 4a. The PL intensity of the perovskite film incorporation with 0.5% potassium ions drops significantly in contrast to other perovskite films, suggesting the excitons can separate and transfer rapidly from perovskite film into TiO_2 layer. The PL intensity of perovskite film doped with potassium ions 1.0% is the highest and most conspicuous, which may result from excess doping ions or the effect of recrystallization. The existence of a large number of grain boundaries and defects in perovskite film (with 1.0% potassium ions) hinders the rapid transfer of excitons. Time-resolved PL (TR-PL) measurements shown in Fig. 4b were carried out on thin films prepared on FTO glasses/compacting TiO_2/mesoporous TiO_2 substrates. The life time of electrons is showed in Table S2. The decay time of 0.66 ns and 6.17 ns in perovskite incorporation with 0.5% potassium ions and pristine perovskite are evaluated using a fitting analysis for the PL decay curves. The shorter PL decay time of perovskite incorporation with 0.5% potassium ions compared to that in pristine perovskite film is consistent with the experimentally observed steady-state PL. The PL decay time drastically decreased in the perovskite incorporation with 0.5% potassium ions due to efficient charge extraction from the perovskite layer. This improvement in exciton transfer and separate might reduce the J–V hysteresis by avoiding the formation of interface capacitance or accumulated charge [28].

The photoelectric conversion characteristics of the fabricated devices are further investigated by measuring their IPCE revealed in Fig. 5a, b. The best device shown in Fig. 5a displays a very broad plateau of IPCE that is over 70%, between 370 and 620 nm. The IPCE of different devices in the short wavelength region (~ 350 nm) are similar. The

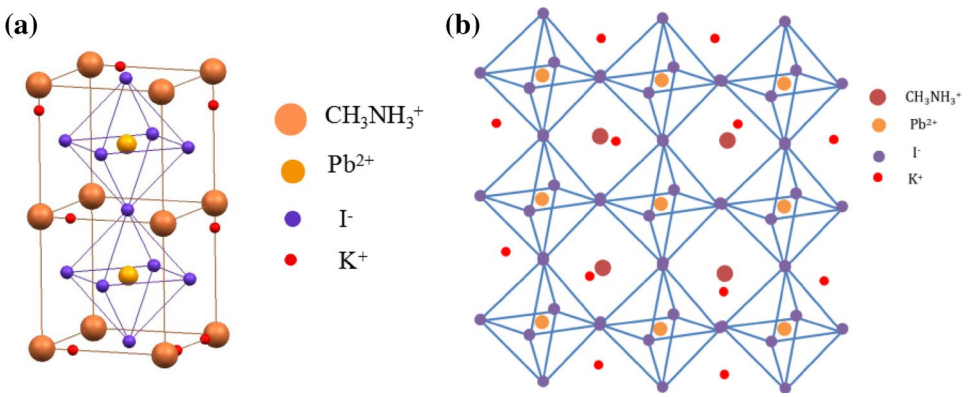

Fig. 2 Illustration of position of K^+ in perovskite structure. **a** Three-dimensional model. **b** Two-dimensional model

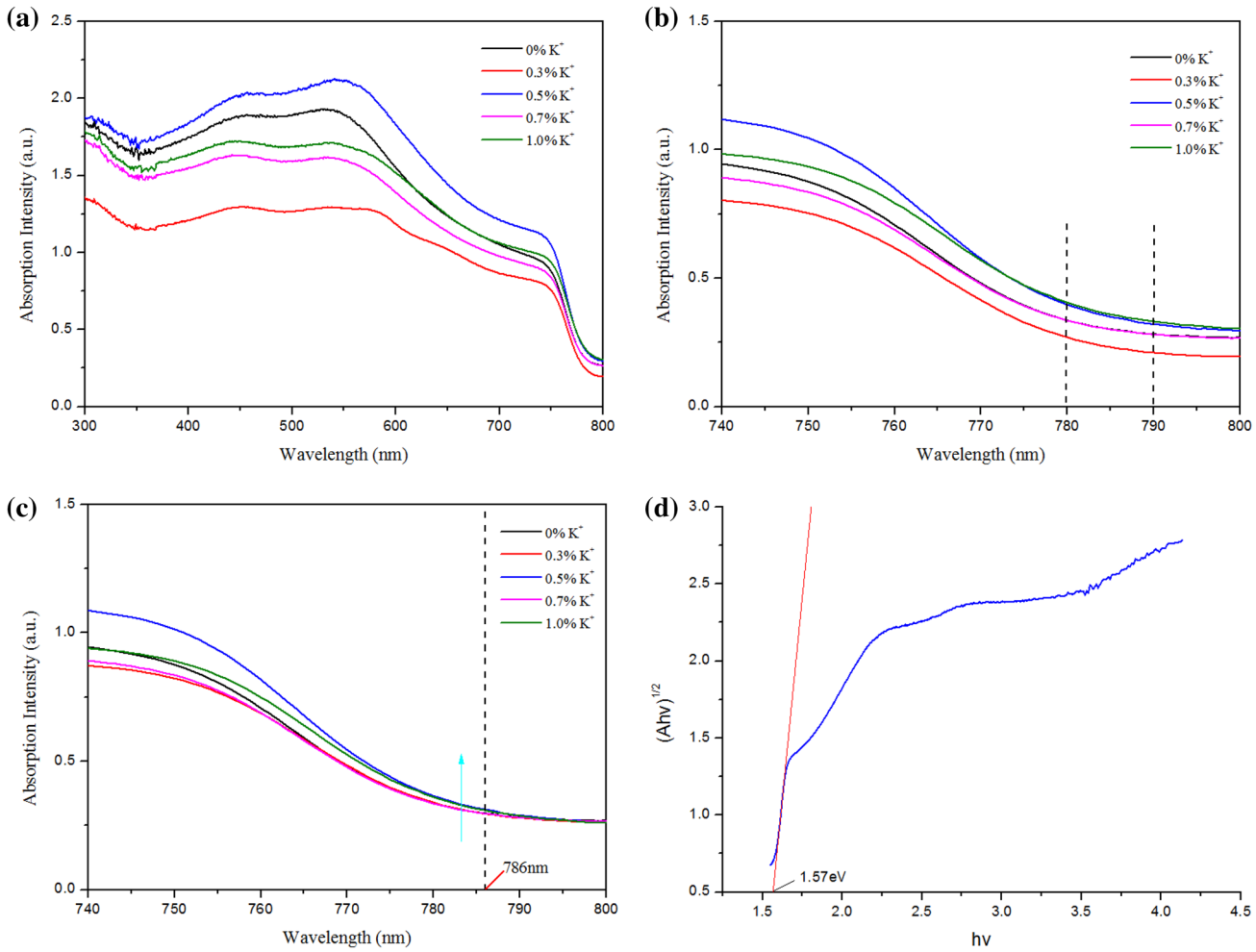

Fig. 3 **a** UV–visible absorption spectra of perovskite film. **b** Absorption spectra magnified in the region ranging from 740 to 800 nm. **c** Absorption spectra at the same right endpoint point. **d** hv–$(Ahv)^{1/2}$ curve of perovskite doped with K^+ (0.5%)

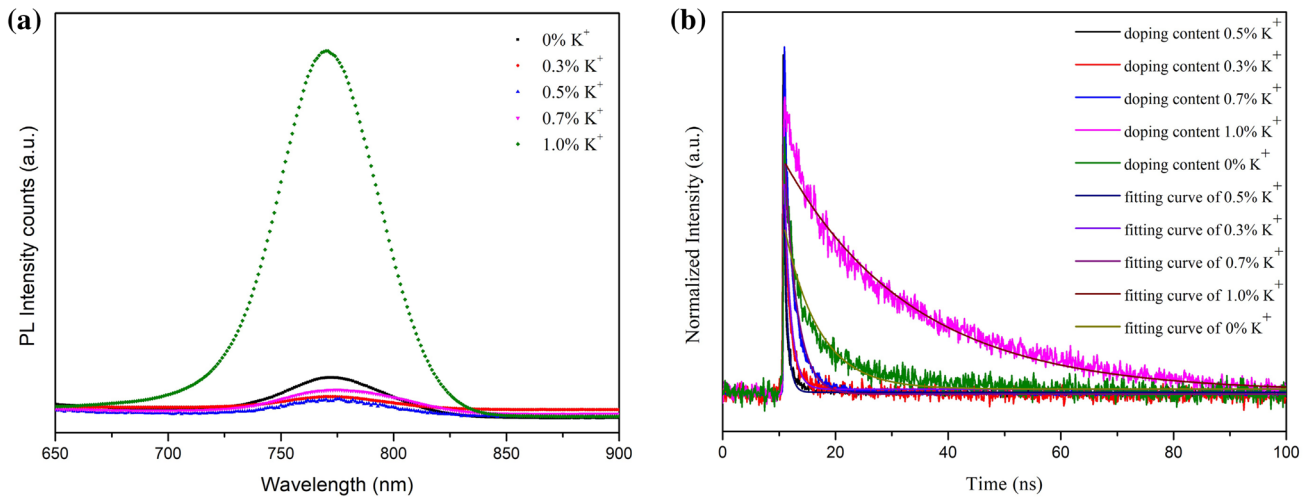

Fig. 4 **a** Steady-state PL spectra and **b** time-resolved PL spectra of the perovskite layers doped with different K^+ contents

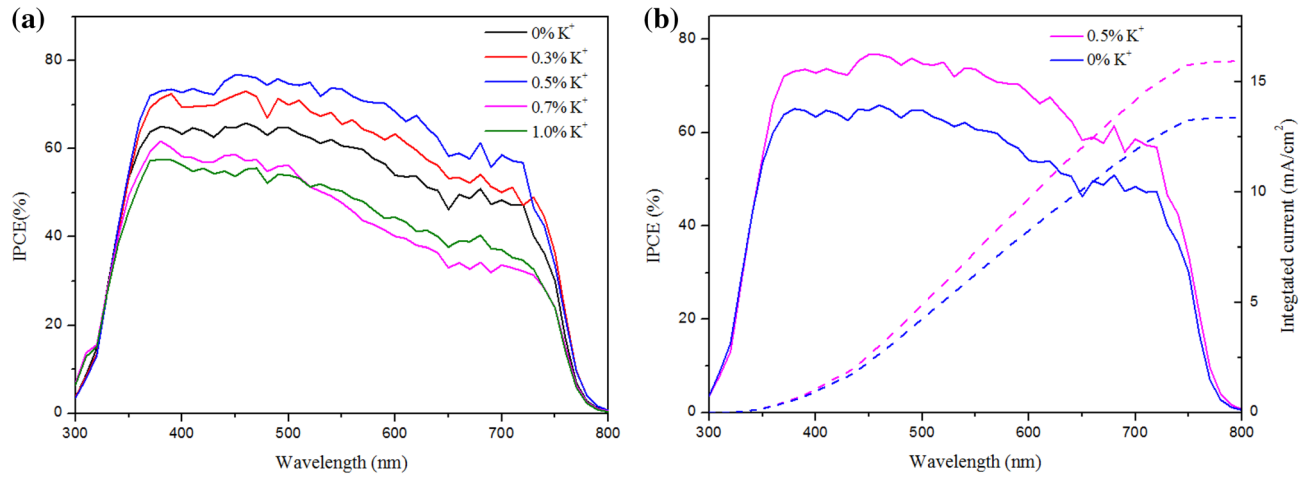

Fig. 5 **a** IPCE spectra of the perovskite devices with different doping content of potassium ions (0–1.0%). **b** Spectra of integrated photocurrents of perovskite devices (0% and 0.5%). The integrated photocurrents (dashed lines) calculated from the overlap integral of the IPCE spectra

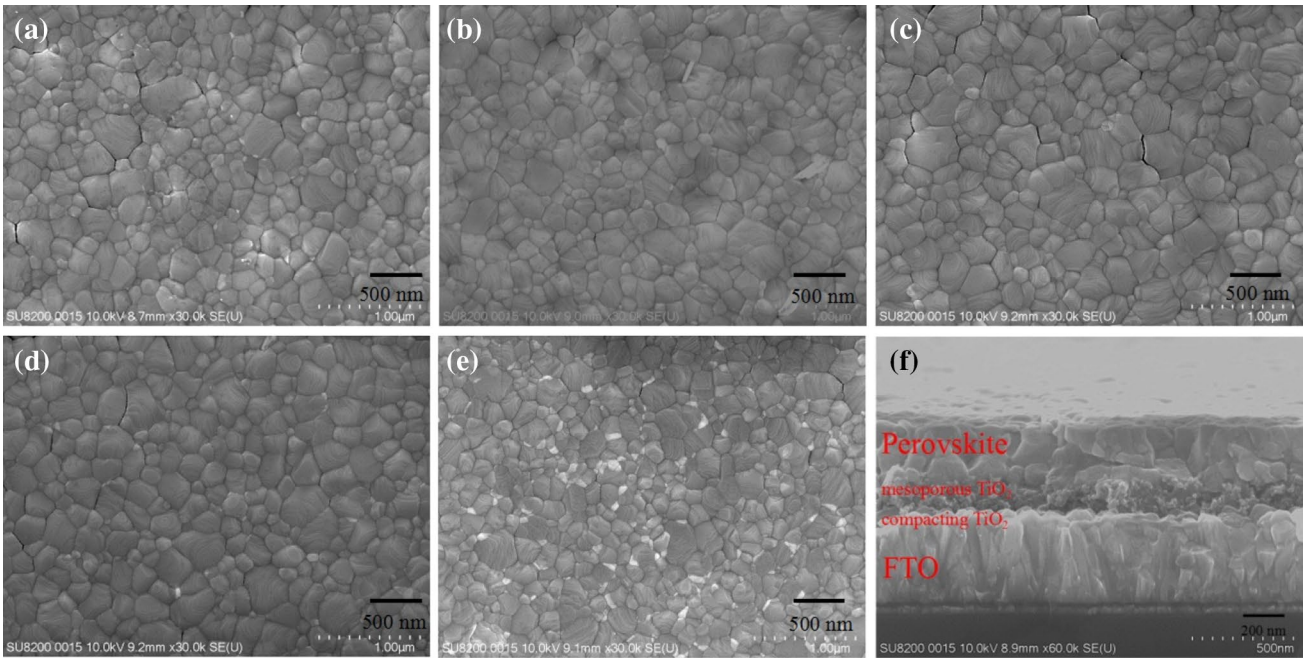

Fig. 6 SEM images of perovskite perovskite films. **a–e** corresponding to doping levels 0%, 0.3%, 0.5%, 0.7%, 1.0%. **f** Cross-sectional SEM image of perovskite film with K^+ (0.5%)

main reason is that the light-harvesting efficiency is nearly saturated due to the high absorbance of perovskite in the short wavelength region [29]. The photo-to-electron quantum efficiency of the wavelength range from 450 to 770 nm shows significant difference and there is a distinct increase for the device prepared with perovskite film that is doped with K^+ (0.5%). The denser perovskite film and enhanced light-harvesting capability have been considered as one reason. In Fig. 4b, integrating the IPCE over the AM 1.5 solar spectrums at 100 mW cm^{-2} irradiance displays estimated J_{sc} of 15.95 and 13.39 mA cm^{-2} for the K^+ (0.5%) doped and control device, respectively. There is tiny discrepancy between the integrated current and measured J_{sc} under the solar simulator due to measurement accuracy and measurement atmosphere. We used two different rigs with two different calibration diodes and these cells were tested in air (humidity 45% RH) without encapsulation, which usually degraded the performance.

The morphology of perovskite thin film with different doping concentrations of potassium ions on FTO glasses/

compacting TiO_2/mesoporous TiO_2 substrates was further investigated by field-emission scanning electron microscopy. As shown in Fig. 6, all the perovskite films are uniform with large regular crystallites, and they cover the underlying layer fully. With the increase of doping concentration (from 0.3 to 0.7%), the grain size shown from Fig. 6b–d increases continuously. The perovskite films have better crystallisation with resultantly fewer crystal defects, which is consistent with XRD measurements shown in Fig. 1. The phenomenon that grain size become larger after doping a small amount of alkaline metal ions in the perovskite growth solution was also reported in the previous literature [25]. The change in grain size may be ascribed to reduced microstrain of perovskite film after doping little alkaline metal ions. According to report, the presence of impurity metal ions during the perovskite crystallization, part ions are expelled to the surface and grain boundaries, giving rise to the reduce of microstrain and crystal defects [23]. With the doping concentration further increasing to 1.0%, a large number of fine grains and grain boundaries appear on the surface of the perovskite film. As we all know, grain boundaries play as recombination centers, which implies the photo generated charges are difficult to reach the corresponding electrode interfaces during transmission process. Note that, some dots with size of tens of nanometers on the surface appearance, especially around grain boundaries. It is highly suspected that the tiny dots are cell grains that act as crystallization cores of perovskite, or residual potassium ions. These residual potassium ions are not crystallization cores and are expelled to the surface and grain boundaries during crystallisation. These potassium ions that located at the grain boundaries can accelerate crystal growth due to heterogeneous nucleation, resulting in narrow grain boundaries filled with fine cell-like grains [30–32]. Based on the above proposed mechanism of perovskite growth mode and influence of potassium ions, a theoretical model is schematically illustrated in Fig. 7.

To further investigate the location and distribution of the potassium ions in the perovskite film, Electron probe microanalyzer (EPMA) was employed to perform elemental mapping for the doping level of 1.0%. The analysis of EPMA is at a surface region which is around 12 μm × 9 μm and the sample is prepared on FTO glasses/compacting TiO_2/mesoporous TiO_2 substrate. The sample of perovskite prepared with the additives displays core level peaks for Pb, I, C, Si, Ti and Sn. The specific content of the various elements is shown in Table S3. Figure 8 illustrates the distribution and relative quantity of potassium ions. The homogeneous distribution of potassium element reveals that one-step method

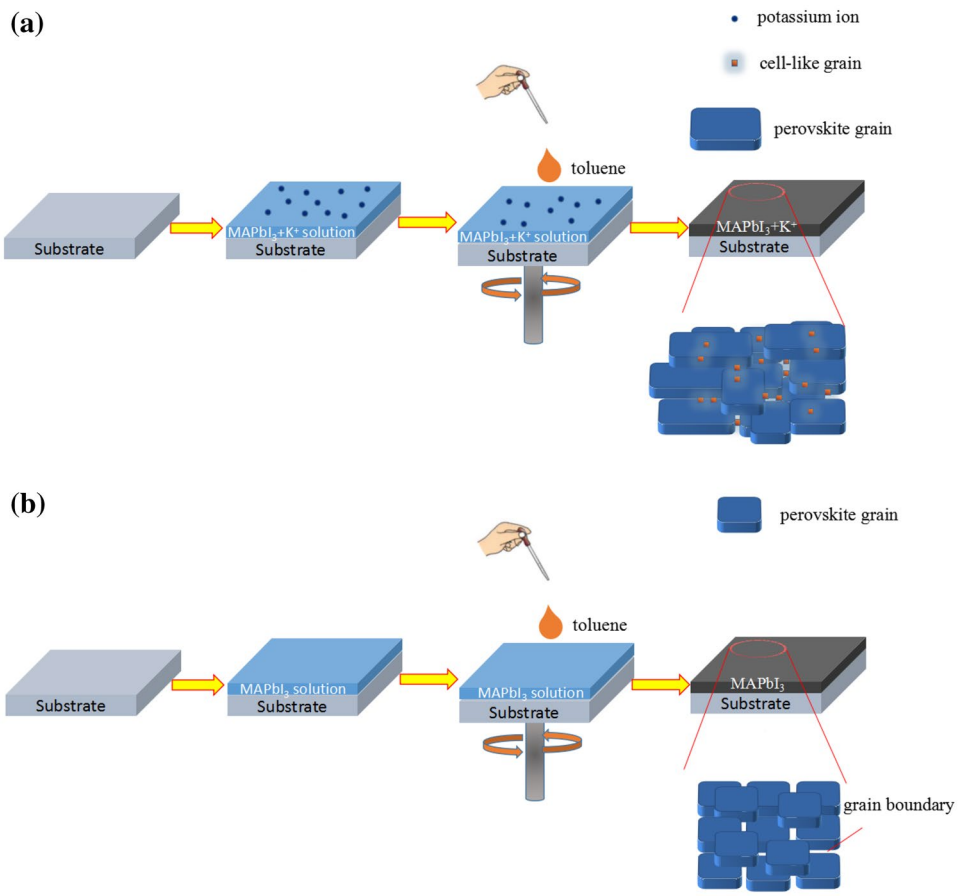

Fig. 7 Theoretical model of fabrication process of perovskite film. **a** Larger grain size and grain boundaries filled with fine cell-like grains of perovskite film after doping potassium ions. **b** Smaller grain size and wider grain boundaries on the film without doping process

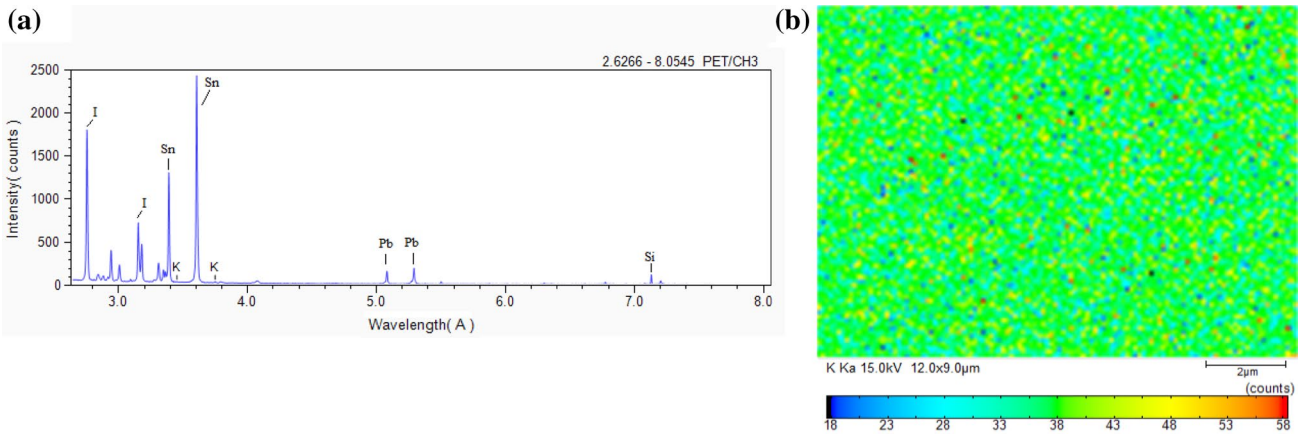

Fig. 8 **a** Relative content of potassium element in perovskite film. **b** Distribution of potassium element in perovskite film

Table 1 Photovoltaic properties of solar cells made with the range of K^+ doping concentrations up to 1.0%

K^+ doped content (%)	J_{sc} (mA cm^{-2})	V_{oc} (V)	FF (%)	PCE (%)
0	14.73	0.99	69.87	10.16
0.3	18.88	0.98	66.14	12.26
0.5	19.98	1.02	66.29	13.57
0.7	19.27	0.98	65.99	12.51
1.0	16.71	0.99	68.05	11.25

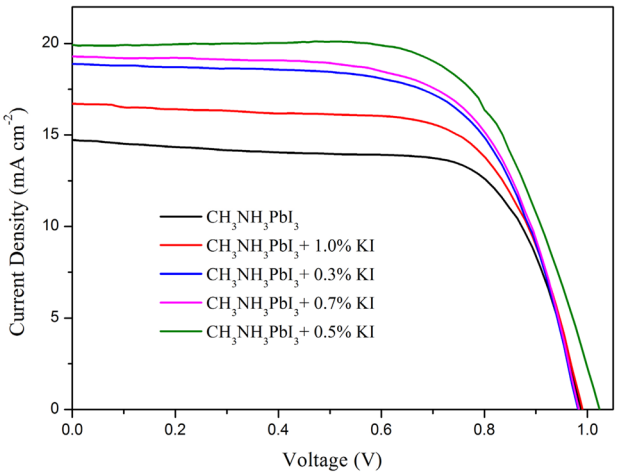

Fig. 9 J–V curves for perovskite cell with different doping content measured by reverse scans with 10 mV voltage steps and 40 ms delay times under AM 1.5G illumination

used in this process is appropriate to prepare uniformly distributed perovskite films based on mesoporous structure. Besides, XPS analysis was used to confirm the existence and state of potassium ions in perovskite film. The survey XPS spectrum and the K2p scan spectrum for the perovskite incorporation with 1.0% potassium ions are shown in Fig. S2. It is obvious that K 2*p* peaks appeared in 292.8 eV and 295.6 eV.

Perovskite solar cells with a FTO/compacting-TiO_2/mesoporous-TiO_2/perovskite/spiro-OMeTAD/Ag structure were fabricated based on the one-step method. The photovoltaic performance of perovskite solar cells with different doping content of potassium ions is shown in Table 1. The characteristic J–V curves are shown in Fig. 9, the device prepared with 0.5% KI achieves the highest PCE (13.57%) and the highest short-circuit current density (J_{sc}) of 19.98 mA cm^{-2}. From Table 1, the case where the addition amount of K^+ is not over 0.5%, the J_{sc} increases gradually as the raise of the doping content of K^+. The improvement of J_{sc} is attributed to the larger grain size, denser perovskite film and less grain boundaries. It has been reported that alkali metal halide additives can act as electrically active impurities that recrystallize the small grains, passivate the grain boundaries and interface states [24]. When the addition content of K^+ is more than 0.5%, the J_{sc} decreases gradually because of the reduced grain size and excess doping ions which act as defect center leading to a great deal of recombination of electrons and holes. It shows that the incorporation of potassium ions into perovskite affects the J_{sc} of PSCs significantly. The result is consistent with conclusion reported in the literature [25]. The V_{oc} value has no distinct increase after potassium ions are doped into perovskite. The reason is that the V_{oc} mainly determined by the band gap value without obvious hole on the film surface. Perovskite with higher band gap values requires higher energy electrons to generate excitation, causing higher V_{oc} value of PSCs. Based on previous UV–vis analysis, the incorporation of potassium ions into perovskite has no tempestuous effect on the band gap value, therefore, the V_{oc} value has no apparent discrepancy. Moreover, histograms of current density and

efficiency of devices doped with 0.5% potassium ions are shown in Fig. S3.

The stability of perovskite solar cells is a critical concern affecting practical application. According to previous report, the incorporation of potassium ions helps to stabilize the perovskite crystals [33]. In the present case, we also found that the device prepared with the K^+ additive was more stable than the device prepared without the additive. As exhibited in Fig. 10a, the stability test indicates that the PCE of the device with K^+ (0.5%) doped maintains 32% after exposing for 18 days. However, the device without potassium ions retains 20% after exposing for 18 days. The reason is the formation of a more compact film with larger crystallites shown in Fig. 6. These unencapsulated devices were stored in a glove box (oxygen: 10 ppm; water: 0.1 ppm) for 18 days and then their performances were tested every 2 days. These devices were charactered in air conditions with 46 RH% for half an hour. The degradation of PCE might arise from the damaged Ag layer and high humidity air condition during test. The Ag layer will be worn out in the fifth times, and the 45 nm thick Ag was deposited on top of the previous Ag layer by thermal evaporation before the sixth test.

Hysteresis in J–V curves of the PSCs was also studied. Hysteresis mainly originated from the defects and the carrier trapping, capacitive effects [34, 35], ferroelectricity, and ion migration [36, 37]. As shown in Fig. 10b, there is no significant hysteresis for the forward and reverse J–V curves of the best performing device. The device parameters (FF, J_{sc}, V_{oc} and PCE) are almost the same along the two scanning directions with different scan rates. The hysteresis index (HI) is 0.03, which is calculated from equation reported in literature [38]: $HI = [J_R(0.8V_{oc}) - J_F(0.8V_{oc})]/J_R(0.8V_{oc})$, where $J_R(0.8V_{oc})$ and $J_F(0.8V_{oc})$ are photocurrent values for the reverse and forward scans at 80% of V_{oc} value. However, the hysteresis index of device without doped potassium ions is 0.1. The forward and reverse J–V curves of control device is shown in Fig. S4. The negligible hysteresis is attributed to the high quality of the perovskite crystals, high charge conductivity and the possible passivation effect from the incorporation of K^+. Zhong et al. has reported that the charge conductivity increased and trap density reduced with the incorporation of potassium ions. The carries have more fast carrier transport speed in the K-containing perovskite films [32]. The solar cells with K^+ doped have less surface shallow trap states and longer charge carrier lifetime compared to the device without K^+ doped by report [39].

4 Conclusions

In conclusion, we have demonstrated the effects of potassium ions doped on the structure, properties of perovskite films and the photovoltaic performance of PSCs. The grain size increased and the perovskite film would be denser with optimal doping levels of 0.5%. For the photovoltaic performance, the J_{sc} can improve obviously while the V_{oc} has no magnificent enhance after doping process. These results reveal that potassium ions can eliminate hysteresis and enhance stable ability of device. This approach using impurity ions into perovskite precursor solutions opens up a new and convenient path to improve the photovoltaic performance of PSCs.

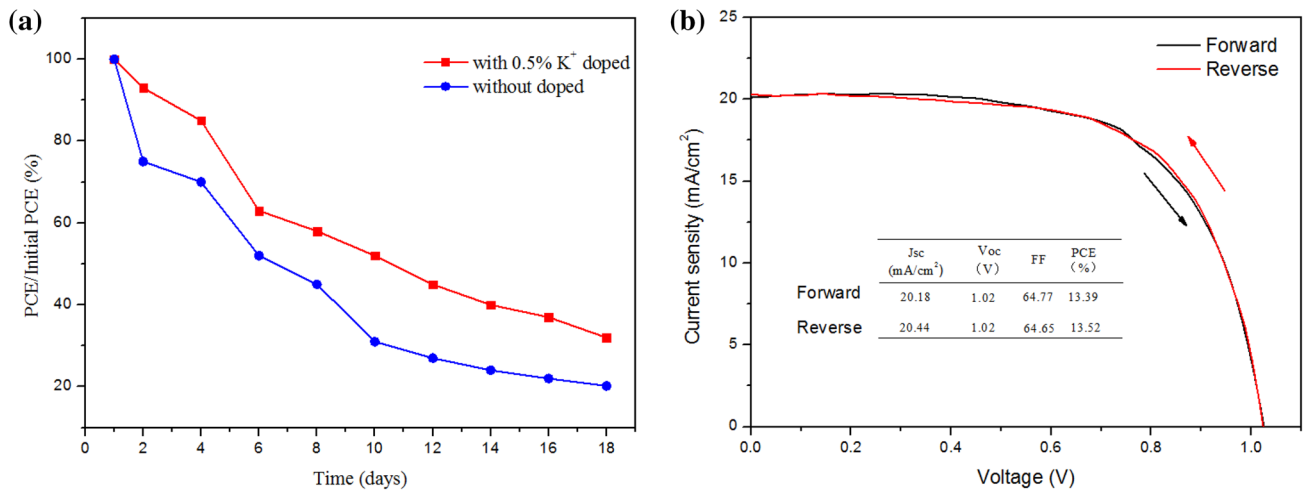

Fig. 10 **a** The relative PCE variation of devices. **b** Forward and reverse J–V curves of PSCs incorporation with K^+ (0.5%)

Acknowledgements This work was financially supported by the Fundamental Research Funds for the Central Universities (Grant No. 2015XKMS067).

References

1. G. Xing, N. Mathews, S. Sun, S.S. Lim, Y.M. Lam, Science **342**, 344 (2013)
2. Z. Huanping, C. Qi, L. Gang, Science **345**, 542 (2014)
3. H. Zhou, Y. Shi, Q. Dong, H. Zhang, Y. Xing, J. Phys. Chem. Lett. **5**, 3241 (2014)
4. S. Colella, E. Mosconi, P. Fedeli, A. Listorti, A. Rizzo, J. Chem. Mater. **25**, 4613 (2013)
5. P.C. Jr, T.J. Savenije, M. Abdellah, J. Am. Chem. Soc. **136**, 5189 (2014)
6. B. NREL, http://www.nrel.gov/ncpv/images/efficiency-chart.jpg, 2016
7. O. Malinkiewicz, A. Yella, H.L. Yong, Nat. Photonics. **8**, 128 (2014)
8. F. Isikgor, B. Li, H. Zhu, J. Mater. Chem. A. (2016). https://doi.org/10.1039/c6ta03381d
9. N.J. Jeon, J.H. Noh, W.S. Yang, Nature **517**, 476 (2015)
10. W.S. Yang, J.H. Noh, N.J. Jeon, Science **348**, 1234 (2015)
11. J. Shi, Y. Luo, H. Wei, ACS. Appl. Mater. Interfaces. **6**, 9711 (2014)
12. M.J. Carnie, C. Charbonneau, M.L. Davies, Chem. Commun. **49**, 7893 (2013)
13. Y. Ogomi, A. Morita, S. Tsukamoto, J. Phys. Chem. Lett. **5**, 1004 (2014)
14. F. Hao, C.C. Stoumpos, R.P.H. Chang, J. Am. Chem. Soc. **45**, 8094 (2014)
15. X.K. Xin, M. He, W. Han, J. Jung, Z.Q. Lin, Angew. Chem. Int. Ed. **50**, 11739 (2011)
16. P.C. Dai, G. Zhang, Y.C. Chen, H.C. Jiang, Z.Y. Feng, Z.J. Lin, J.H. Zhan, Chem. Commun. **48**, 3006 (2012)
17. N. Pellet, P. Gao, G. Gregori, T.Y. Yang, M.K. Nazeeruddin, Angew. Chem. Int. Ed. **53**, 3151 (2014)
18. Y. Zhou, M. Yang, S. Pang, K. Zhu, K.N.P. Padture, J. Am. Chem. Soc. **138**, 5535 (2016)
19. D. Stranks, G.E. Eperon, G. Grancini, C. Menelaou, M.J. Alcocer, Science. **342**, 341 (2013)
20. N. Pellet, P. Gao, G. Gregori, Angew. Chem. **53**, 3151 (2014)
21. N.K. Noel, S.D. Stranks, A. Abate, Energy Environ. Sci. **7**, 3061 (2014)
22. X. Zhang, X. Ren, B. Liu, Energy Environ. Sci. **10**, 2095–2102 (2017)
23. T.W. Wang, Z. Wang, S. Pathak, Energy Environ. Sci. **9**, 2892–2901 (2016)
24. K.M. Boopathi, R. Mohan, T.Y. Huang, J. Mater. Chem. A. **4**, 1591 (2016)
25. J. Chang, Z. Lin, H. Zhu, F.H. Isikgor, J. Mater. Chem. A. **4**, 16546 (2016)
26. N.J. Jeon, J.H. Noh, Y.C. Kim, Nat. Mater. **13**, 897 (2014)
27. T.C. Steven, Ferroelectrics. **470**, 13 (2014)
28. J.H. Heo, M.S. You, M.H. Chang, Nano Energy **15**, 530 (2015)
29. Y. Huang, J. Zhu, Y. Ding, ACS Appl. Mater. Interfaces **8**, 8162 (2016)
30. N. Kubota, J.W. Mullin, J. Cryst. Growth **152**, 203 (1995)
31. K. Sangwal, J. Cryst. Growth **203**, 197 (1999)
32. J.J. De Yoreo, P.U. Gilbert, N.A. Sommerdijk, Science. **349**, 6760 (2015)
33. T. Bu, X. Liu, Y. Zhou, Energy Environ. Sci. **10**, 2509–2515 (2017)
34. T.J. Jacobsson, J.P. Correabaena, E.H. Anaraki, J. Am. Chem. Soc. **138**, 10331 (2016)
35. B. Chen, M. Yang, S. Priya, J. Phys. Chem. Lett. **7**, 905 (2016)
36. H.W. Chen, N. Sakai, M. Ikegami, J. Phys. Chem. Lett. **6**, 164 (2015)
37. A. Dualeh, T. Moehl, N. Tetreault, ACS Nano. **8**, 362 (2014)
38. T.P. Gujar, T. Unger, A. Schönleber, Phys. Chem. Chem. Phys. **20**, 605 (2017)
39. D. Yao, C. Zhang, N.D. Pham, J. Phys. Chem. Lett. **9**, 2113 (2018)